Eur. Phys. J. C (2019) 79:1025
https://doi.org/10.1140/epjc/s10052-019-7543-4

THE EUROPEAN PHYSICAL JOURNAL C

Regular Article - Theoretical Physics

Molecular Ξ_{bc} states from meson–baryon interaction

Qi-Xin Yu[1,2,a], **J. M. Dias**[1,3,b], **Wei-Hong Liang**[1,4,c], **E. Oset**[1,5,d]

[1] Department of Physics, Guangxi Normal University, Guilin 541004, China
[2] Institute for Experimental Physics, Department of Physics, University of Hamburg, Luruper Chaussee 149, 22761 Hamburg, Germany
[3] Instituto de Física, Universidade de São Paulo, Rua do Matão 1371, Butantã, São Paulo, São Paulo CEP 05508-090, Brazil
[4] Guangxi Key Laboratory of Nuclear Physics and Technology, Guangxi Normal University, Guilin 541004, China
[5] Departamento de Física Teórica and IFIC, Centro Mixto Universidad de Valencia-CSIC Institutos de Investigación de Paterna, Aptdo. 22085, 46071 Valencia, Spain

Received: 7 October 2019 / Accepted: 8 December 2019 / Published online: 21 December 2019

Abstract We have studied the meson–baryon interaction in coupled channels with the same quantum numbers of Ξ_{bc}. The interaction is attractive in some channels and of sufficient intensity to lead to bound states or resonances. We use a model describing the meson–baryon interaction based on an extrapolation of the local hidden gauge approach to the heavy sector, which has been successfully used in predicting Ω_c and hidden charm states. We obtain many states, some of them narrow or with zero width, as a consequence of the interaction, which qualify as molecular states in those channels. The success in related sectors of the picture used should encourage the experimental search for such states.

1 Introduction

The spectroscopy of baryons with heavy quarks has raised a wave of intensive theoretical work, with models competing to explain experimental facts and make new predictions. The reporting of several pentaquark states in Ref. [1], updated recently [2], was a main trigger of this wave of works, but other works, as the discovery of several narrow Ω_c states [3], and the more recent finding of a Ξ_{cc}^{++} state [4], have also contributed to keep the flame alive.

The Ξ_{cc}^{++} discovery was again a turning point, since previous theoretical works had made predictions for its existence [5–7] (see further information in Ref. [8]). After the experimental discovery [4] the attention to doubly heavy baryons experienced a boom and those states have been considered from various points of view. Much of the attention has been given to weak decays of these states [9–26], but strong and electromagnetic decays also received some attention [27–32]. Magnetic moments of these states have also been evaluated in different approaches [33–36]. Concerning masses and spectra of excited states, sum rules have contributed their share, with the customary large uncertainties [19,37–40], and have also been used to evaluate weak decays [41,42]. Lattice QCD calculations have also been done for the ground states [43]. As usual, quark models have been also used, mostly from the conventional QQq structure, to obtain spectra of doubly heavy baryons [44–51]. Detailed spectra for Ξ_{cc} and Ξ_{bc} states, among others, are obtained in Ref. [52] using the hypercentral constituent quark model. Heavy quark spin symmetry has also been one of the elements used to obtain spectra of doubly heavy baryons relating the different heavy flavor sectors [53–55].

Related works include the study of systems of a light pseudoscalar with doubly heavy baryons [56–58], studies of triple charm molecular pentaquarks of $\Xi_{cc}D^{(*)}$ systems with pion exchange [59], the use of Lorentz-invariant baryon chiral perturbation theory to study the ground state of Ξ_{cc} [60], the study of electromagnetic form factors of Ξ_{cc}, Ω_{cc} [61], and the study of Ξ_{cc}, Ξ_{bc} and Ξ'_{bc} masses using a scalar confining potential and one gluon exchange with the Bethe–Salpeter equation [62]. Reviews on these topics can be found in Refs. [63–65]. Related to the works of Refs. [56–58] is the work of Ref. [66], but with more coupled channels. For instance, in addition to $\Xi_{cc}\pi$, $\Xi_{cc}\eta$, $\Omega_{cc}K$, that account for a light pseudoscalar and a heavy baryon, the $\Lambda_c D$, $\Sigma_c D$, $\Xi_c D_s$, $\Xi'_c D_s$ channels are considered to produce Ξ_{cc} states in $J^P = 1/2^-$, which by themselves give rise to molecular states. Similar states using vector–baryon interaction and mesons with $3/2^+$ baryons are also considered in Ref. [66]. The approach predicts several states of negative parity between 3837 MeV and 4374 MeV. It is clear that

[a] e-mail: yuqx@mail.bnu.edu.cn
[b] e-mail: isengardjor@gmail.com
[c] e-mail: liangwh@gxnu.edu.cn
[d] e-mail: oset@ific.uv.es

when including coupled channels with charmed mesons one can no longer invoke chiral dynamics, as is the case when dealing with light pseudoscalar in Refs. [56–58]. Instead, a method was found in Refs. [67,68] to produce a reliable source of interaction in this case:

(i) First one realizes that the chiral Lagrangians in SU(3) can be obtained from the local hidden gauge approach [69–72] by exchanging vector mesons. This was shown in the case of the pseudoscalar-pseudoscalar interaction in Ref. [73].
(ii) Take a typical channel $\Xi_c D$ and the direct transition $\Xi_c D \to \Xi_c D$. The D^+ flavor wave function is just $c\bar{d}$, and for the Ξ_c and other baryons we single out the heavy quark and impose flavor-spin symmetry in the remaining light quarks. Thus, explicitly one is not making use of SU(4) symmetry. The direct $\Xi_c D \to \Xi_c D$ transition is mediated by the exchange of light vectors and c quarks in D and Ξ_c act as spectators. Then the interaction follows the SU(3) symmetry of the light quarks. A welcome side effect is that, since the heavy quarks are spectators, the interaction does not depend upon them and heavy quark symmetry is automatically implemented.
(iii) Some non-diagonal transitions, like $\Sigma_c D \to \Xi_{cc}\pi$, require the exchange of a D^* and here the heavy quarks are no longer spectators. Yet, no SU(4) is used in the approach with the wave functions used, and the vertices VPP, VBB (V for vector, P for pseudoscalar and B for baryon) essentially count the number of quarks involved in the exchange. Yet, these terms no longer comply with heavy quark symmetry, as one finds explicitly, but neither should they, since the interaction goes as $\mathcal{O}(\frac{1}{m_Q^2})$ (m_Q for the mass of the heavy quark) from the D^* propagator, and these terms are subleading in the $\mathcal{O}(\frac{1}{m_Q})$ counting, and small in practice.
(iv) One needs a piece of experimental information to fine tune the regulator of the loops (usually $q_{\max}$ for the modulus of the three momentum), which is adjusted to some mass and should be of natural size in the range of 600–800 MeV. Then the masses and widths of many states are predicted by the approach.

This said it is not surprising that the approaches which use explicitly SU(4) for the evaluation of this interaction obtain the same results for the transition matrix elements led by the exchange of light vectors, since automatically they are effectively using the SU(3) subgroup of this group. This is the case of the work of Ref. [74] in the study of Ω_c molecular states. There are differences with respect to Ref. [67] in the transitions including the exchange of heavy vectors, but since this interaction is small, it is not surprising that in the end the results of Ref. [74] using SU(4) and those of Ref. [67] where SU(4) is not used, are very similar.

The approach described above has been very successful, and in Ref. [67] three of the Ω_c states of Ref. [3] were correctly reproduced in mass and width. In Ref. [75] heavy quark spin symmetry (HQSS) was used to find the relationship between the transition matrix elements of the coupled channels, $\bar{D}^{(*)}\Sigma_c^{(*)}$, $J/\psi N$ and others, to describe the recent hidden charm pentaquark states [2]. The strength of the interaction was obtained from the evaluation of the hidden gauge approach described above. Once again, the states found in the experiment were fairly well reproduced and a few more states were predicted. These results are similar to those of Ref. [76], where also HQSS is used to evaluate masses, but in addition the widths are evaluated in Ref. [67].

The approach of Ref. [67] to study the Ω_c states is also used in Ref. [66] in the study of the Ξ_{cc} states, in Ref. [77] in the study of Ξ_c and Ξ_b states and in Ref. [78] in the study of Ω_b states.

In the present work we study in detail the Ξ_{bc} states that can emerge from the interaction of pseudoscalar-baryon $(1/2^+)$ interaction, vector–baryon $(1/2^+)$ interaction and pseudoscalar-baryon $(3/2^+)$ interaction. Using the same regulator obtained in cases where we could contrast with experiment, and the same source of information, we obtain several states in each sector. We evaluate binding energies and widths, as well as couplings of the resonant states to the different channels. In some cases we can see a striking dominance of one of the channels, which allows us to deem the state as a molecular state of this channel. Since we work in meson–baryon interaction in s-wave, we also evaluate the wave functions at the origin for the different channels, which provide extra information concerning the relevance of the channels in different reactions.

2 Formalism

2.1 Baryon states

In order to see the coupled channels that we need, we classify the meson–baryon states as

(1) Meson–baryon states with both b and c quarks in the baryon. For this case, we have baryons: $\Xi_{bc} \equiv bcq$ (q for u or d quark); $\Omega_{bc} \equiv bcs$. The coupled channels of pseudoscalar meson and baryon are

$$\pi\,\Xi_{bc}, \quad \eta\,\Xi_{bc}, \quad K\,\Omega_{bc}; \tag{1}$$

(2) Meson–baryon states with b in the baryon and c in the meson. The coupled channels are

$$D\Lambda_b, \quad D\Sigma_b, \quad D_s\,\Xi_b, \quad D_s\,\Xi_b'; \tag{2}$$

Table 1 Wave functions for baryons with $J^P = 1/2^+$ and $I = 0, 1/2, 1$. MS and MA stand for mixed symmetric and mixed antisymmetric, respectively

States	I, J	Flavor	Spin
Ω_{bc}^0	$0, 1/2$	bcs	χ_{MS}, χ_{MA}
Λ_b^0	$0, 1/2$	$\frac{b}{\sqrt{2}}(ud-du)$	χ_{MA}
Σ_b^+	$1, 1/2$	$\frac{1}{\sqrt{2}}buu$	χ_{MS}
Ξ_b^0	$1/2, 1/2$	$\frac{b}{\sqrt{2}}(us-su)$	χ_{MA}
$\Xi_b^{\prime 0}$	$1/2, 1/2$	$\frac{b}{\sqrt{2}}(us+su)$	χ_{MS}
Λ_c^+	$0, 1/2$	$\frac{c}{\sqrt{2}}(ud-du)$	χ_{MA}
Σ_c^{++}	$1, 1/2$	cuu	χ_{MS}
Ξ_c^+	$1/2, 1/2$	$\frac{c}{\sqrt{2}}(us-su)$	χ_{MA}
$\Xi_c^{\prime 0}$	$1/2, 1/2$	$\frac{c}{\sqrt{2}}(us+su)$	χ_{MS}

Table 2 Wave functions for baryons with $J^P = 3/2^+$ and $I = 0, 1/2, 1$. S in χ_S stands for full symmetric

States	I, J	Flavor	Spin
Ω_{bc}^{*0}	$0, 3/2$	bcs	χ_S
Σ_b^{*+}	$1, 3/2$	buu	χ_S
Ξ_b^{*0}	$1/2, 3/2$	$\frac{b}{\sqrt{2}}(us+su)$	χ_S
Σ_c^{*++}	$1, 3/2$	cuu	χ_S
Ξ_c^{*+}	$1/2, 3/2$	$\frac{c}{\sqrt{2}}(us+su)$	χ_S

(3) Meson–baryon states with c in the baryon and b in the meson. The coupled channels are

$$\bar{B}\Lambda_c, \quad \bar{B}\Sigma_c, \quad \bar{B}_s\Xi_c, \quad \bar{B}_s\Xi_c'. \tag{3}$$

Next we take the baryon wave functions isolating the heavy quarks and imposing the spin-flavor symmetry on the light quarks. In our approach it is important to specify the spin of the states because, as we shall see below, the interaction is spin independent, which immediately imposes selection rules in the transitions. The wave functions are summarized in Tables 1 and 2.

The corresponding states with different charge are trivial using the u, d quarks. In Tables 1 and 2 χ_{MS}, χ_{MA}, χ_S are the spin wave functions of the three quarks [79].

In the interaction we exchange vector mesons as shown in Fig. 1. The lower vertex of VBB is of the type $\gamma^\mu\epsilon_\mu$, but, with heavy baryons and close to threshold, only the $\gamma^0 \simeq 1$ term is relevant, which means that this vertex is spin independent, and so is the upper vertex that will go as $(p_D + p'_D)^0$. For $VB \to VB$ transitions, the upper vertex has the same structure, but with the additional $\vec{\epsilon}\cdot\vec{\epsilon}\,'$ factor for the vector polarizations, which is diagonal in the spin of the vectors. With the spin-independent interaction, we can classify the

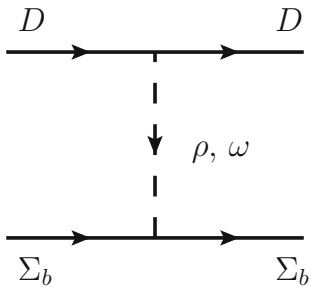

Fig. 1 Example of interaction for one of the channels

meson–baryon channels according to the spin wave functions of baryons, *i.e.*, χ_{MS}, χ_{MA} or χ_S. Hence we have the blocks of coupled channels:

(A) PB channels with χ_{MS} for the baryon: $\pi\Xi_{bc}$, $\eta\Xi_{bc}$, $K\Omega_{bc}$, $D\Sigma_b$, $D_s\Xi_b'$, $\bar{B}\Sigma_c$, $\bar{B}_s\Xi_c'$.
(B) PB channels with χ_{MA} for the baryon: $\pi\Xi_{bc}$, $\eta\Xi_{bc}$, $K\Omega_{bc}$, $D\Lambda_b$, $D_s\Xi_b$, $\bar{B}\Lambda_c$, $\bar{B}_s\Xi_c$.
(C) PB channels with χ_S for the baryon: $\pi\Xi_{bc}^*$, $\eta\Xi_{bc}^*$, $K\Omega_{bc}^*$, $D\Sigma_b^*$, $D_s\Xi_b^*$, $\bar{B}\Sigma_c^*$, $\bar{B}_s\Xi_c^*$.
(D) VB channels with χ_{MS} for the baryon: $\rho\Xi_{bc}$, $\omega\Xi_{bc}$, $\phi\Xi_{bc}$, $K^*\Omega_{bc}$, $D^*\Sigma_b$, $D_s^*\Xi_b'$, $\bar{B}^*\Sigma_c$, $\bar{B}_s^*\Xi_c'$.
(E) VB channels with χ_{MA} for the baryon: $\rho\Xi_{bc}$, $\omega\Xi_{bc}$, $\phi\Xi_{bc}$, $K^*\Omega_{bc}$, $D^*\Lambda_b$, $D_s^*\Xi_b$, $\bar{B}^*\Lambda_c$, $\bar{B}_s^*\Xi_c$.

We do not study the interaction of vectors with $J^P = 3/2^+$ baryons. From previous works the states obtained belong to a region where signals are difficult to see experimentally.

2.2 Isospin states

We take the isospin multiplets:

$$\Xi_{bc} = \begin{pmatrix} \Xi_{bc}^+ \\ \Xi_{bc}^0 \end{pmatrix}, \tag{4}$$

$$D = \begin{pmatrix} D^+ \\ -D^0 \end{pmatrix}, \tag{5}$$

$$\bar{D} = \begin{pmatrix} \bar{D}^0 \\ D^- \end{pmatrix}, \tag{6}$$

$$\Xi_b = \begin{pmatrix} \Xi_b^0 \\ \Xi_b^- \end{pmatrix}, \tag{7}$$

$$\Xi_b' = \begin{pmatrix} \Xi_b^{\prime 0} \\ \Xi_b^{\prime -} \end{pmatrix}, \tag{8}$$

$$B = \begin{pmatrix} B^+ \\ B^0 \end{pmatrix}, \tag{9}$$

$$\bar{B} = \begin{pmatrix} \bar{B}^0 \\ -B^- \end{pmatrix}, \tag{10}$$

$$K = \begin{pmatrix} K^+ \\ K^0 \end{pmatrix}, \tag{11}$$

$$\bar{K} = \begin{pmatrix} \bar{K}^0 \\ -K^- \end{pmatrix}, \tag{12}$$

$$\pi = \begin{pmatrix} -\pi^+ \\ \pi^0 \\ \pi^- \end{pmatrix}, \tag{13}$$

$$\rho = \begin{pmatrix} -\rho^+ \\ \rho^0 \\ \rho^- \end{pmatrix}, \tag{14}$$

$$\Sigma_b = \begin{pmatrix} \Sigma_b^+ \\ \Sigma_b^0 \\ \Sigma_b^- \end{pmatrix}. \tag{15}$$

and the rest are trivial.

2.3 Evaluation of matrix elements

The evaluation of the upper vertex of Fig. 1, VPP, is done in Ref. [68] using the vector character of the vertex and the quark content of the mesons. Yet, it was found that for practical purpose one can get it from the Lagrangian

$$\mathcal{L} = -ig\langle \left[P, \partial_\mu P\right] V^\mu \rangle, \tag{20}$$

where $\langle \cdots \rangle$ stands for the matrix trace, $g = M_V/2f_\pi, M_V = 800\,\text{MeV}$, $f_\pi = 93\,\text{MeV}$ and

$$P = \begin{pmatrix} \frac{1}{\sqrt{2}}\pi^0 + \frac{1}{\sqrt{3}}\eta + \frac{1}{\sqrt{6}}\eta' & \pi^+ & K^+ & \bar{D}^0 \\ \pi^- & -\frac{1}{\sqrt{2}}\pi^0 + \frac{1}{\sqrt{3}}\eta + \frac{1}{\sqrt{6}}\eta' & K^0 & D^- \\ K^- & \bar{K}^0 & -\frac{1}{\sqrt{3}}\eta + \sqrt{\frac{2}{3}}\eta' & D_s^- \\ D^0 & D^+ & D_s^+ & \eta_c \end{pmatrix}, \tag{21}$$

$$V = \begin{pmatrix} \frac{1}{\sqrt{2}}\rho^0 + \frac{1}{\sqrt{2}}\omega & \rho^+ & K^{*+} & \bar{D}^{*0} \\ \rho^- & -\frac{1}{\sqrt{2}}\rho^0 + \frac{1}{\sqrt{2}}\omega & K^{*0} & \bar{D}^{*-} \\ K^{*-} & \bar{K}^{*0} & \phi & D_s^{*-} \\ D^{*0} & D^{*+} & D_s^{*+} & J/\psi \end{pmatrix}, \tag{22}$$

when dealing with charmed mesons, and

$$P = \begin{pmatrix} \frac{1}{\sqrt{2}}\pi^0 + \frac{1}{\sqrt{3}}\eta + \frac{1}{\sqrt{6}}\eta' & \pi^+ & K^+ & B^+ \\ \pi^- & -\frac{1}{\sqrt{2}}\pi^0 + \frac{1}{\sqrt{3}}\eta + \frac{1}{\sqrt{6}}\eta' & K^0 & B^0 \\ K^- & \bar{K}^0 & -\frac{1}{\sqrt{3}}\eta + \sqrt{\frac{2}{3}}\eta' & B_s^0 \\ B^- & \bar{B}^0 & \bar{B}_s^0 & \eta_b \end{pmatrix}, \tag{23}$$

$$V = \begin{pmatrix} \frac{1}{\sqrt{2}}\rho^0 + \frac{1}{\sqrt{2}}\omega & \rho^+ & K^{*+} & B^{*+} \\ \rho^- & -\frac{1}{\sqrt{2}}\rho^0 + \frac{1}{\sqrt{2}}\omega & K^{*0} & B^{*0} \\ K^{*-} & \bar{K}^{*0} & \phi & B_s^{*0} \\ B^{*-} & \bar{B}^{*0} & \bar{B}_s^{*0} & \Upsilon \end{pmatrix}, \tag{24}$$

when dealing with bottomed mesons.

We find the following states classified as BP, BV. For consistency with Ref. [66] we write the states as baryon-meson. Then

$$\left|\Sigma_b D; 1/2, 1/2\right\rangle = -\sqrt{\frac{2}{3}}\left|\Sigma_b^+ D^0\right\rangle - \sqrt{\frac{1}{3}}\left|\Sigma_b^0 D^+\right\rangle, \tag{16}$$

$$\left|\Sigma_c \bar{B}; 1/2, 1/2\right\rangle = -\sqrt{\frac{2}{3}}\left|\Sigma_c^{++} B^-\right\rangle - \sqrt{\frac{1}{3}}\left|\Sigma_c^+ \bar{B}^0\right\rangle, \tag{17}$$

$$\left|\Sigma_b^* D; 1/2, 1/2\right\rangle = -\sqrt{\frac{2}{3}}\left|\Sigma_b^{*+} D^0\right\rangle - \sqrt{\frac{1}{3}}\left|\Sigma_b^{*0} D^+\right\rangle, \tag{18}$$

$$\left|\Sigma_c^* \bar{B}; 1/2, 1/2\right\rangle = -\sqrt{\frac{2}{3}}\left|\Sigma_c^{*++} B^-\right\rangle - \sqrt{\frac{1}{3}}\left|\Sigma_c^{*+} B^0\right\rangle, \tag{19}$$

The lower vertex is trivial to evaluate. The Lagrangian for the VBB vertex is given by the operator

$$\mathcal{L} \to \begin{cases} \frac{g}{\sqrt{2}}(u\bar{u} - d\bar{d}) & \text{for } \rho^0 \\ \frac{g}{\sqrt{2}}(u\bar{u} + d\bar{d}) & \text{for } \omega \end{cases} \tag{25}$$

Hence, for instance, $\rho^0 \Xi_{bc}^0 \Xi_{bc}^0$ involves the vertex

$$\left\langle bcd\right| \frac{g}{\sqrt{2}}(u\bar{u} - d\bar{d}) \left|bcd\right\rangle = -g\frac{1}{\sqrt{2}}. \tag{26}$$

Then we get finally transition matrix elements

$$V_{ij} = D_{ij} \frac{1}{4 f_\pi^2} (k^0 + k'^0), \tag{27}$$

where k^0, k'^0 are the energies of the mesons and D_{ij} the coefficients which are shown in Tables in the next section. With the potential of Eq. (27) we solve the Bethe–Salpeter equation in coupled channels

$$T = [1 - VG]^{-1} V, \tag{28}$$

where G is the meson–baryon loop function

$$\begin{aligned} G_l &= i \int \frac{d^4q}{(2\pi)^4} \frac{M_l}{E_l(\mathbf{q})} \frac{1}{k^0 + p^0 - q^0 - E_l(\mathbf{q}) + i\epsilon} \frac{1}{q^2 - m_l^2 + i\epsilon} \\ &= \int_{|\mathbf{q}|<q_{\max}} \frac{d^3\mathbf{q}}{(2\pi)^3} \frac{1}{2\omega_l(\mathbf{q})} \frac{M_l}{E_l(\mathbf{q})} \frac{1}{k^0 + p^0 - \omega_l(\mathbf{q}) - E_l(\mathbf{q}) + i\epsilon}, \end{aligned} \tag{29}$$

and we use $q_{\max} = 650\,\text{MeV}$ as in Refs. [66,67,78]. ω_l, E_l are the energies of the meson and baryon respectively, $\omega_l = \sqrt{m_l^2 + \mathbf{q}^2}$, $E_l = \sqrt{M_l^2 + \mathbf{q}^2}$, and m_l, M_l the meson and baryon masses. In Eq. (29) p^0 is the energy of the incoming baryon.

In order to get poles in the second Riemann sheet we replace G by G^{II}, and it is given by

$$G_l^{II} = \begin{cases} G_l(s) & \text{for } \text{Re}(\sqrt{s}) < \sqrt{s}_{th,l} \\ G_l(s) + i \dfrac{2M_l q}{4\pi\sqrt{s}} & \text{for } \text{Re}(\sqrt{s}) \geq \sqrt{s}_{th,l} \end{cases}, \tag{30}$$

where $\sqrt{s}_{th,l}$ is the threshold mass of the l channel, and

$$q = \frac{\lambda^{1/2}(s, m_l^2, M_l^2)}{2\sqrt{s}} \quad \text{with } \text{Im(q)} > 0. \tag{31}$$

For the evaluation of the couplings g_l of the state to different coupled channels, we find that the T_{ij} matrix can be expressed in the following form close to the poles, z_R,

$$T_{ij}(s) = \frac{g_i g_j}{\sqrt{s} - z_R}, \tag{32}$$

which defines the couplings g_i up to a global sign of one of them.

The approach followed relies on the exchange of vector mesons, which we justified from the extension of the chiral Lagrangians via the local hidden gauge approach. In meson–baryon interactions the exchange of pseudoscalar mesons is also sometimes used [80], together with σ-exchange. Unlike in baryon–baryon interaction where the π exchange plays a very important role, in meson-meson or meson–baryon interaction, pion exchange plays a more moderate role because the direct $PB \to PB$ through π exchange does not go, since a three-pseudoscalar vertex is forbidden by parity-angular-momentum conservation. It is through intermediate states transitions $PB \to VB \to PB$ that the π-exchange can have a contribution. Detailed calculations of its effects have also been considered in the study of baryon states with open charm [81] and hidden charm [82] and the main source of interaction remains vector exchange. Also, to some extend, the two step process $PB \to VB \to PB$ can be incorporated into an effective transition potential δV for $PB \to PB$, adding to the vector exchange potential, and this extra potential can again be effectively accounted for by changes in the cut off that regularizes the loop function G, since $[V^{-1} - G]$ will be the same with an extra δV and $\delta G = \delta(V^{-1})$. Yet, not all the contributions can be reabsorbed in this way and one may expect some remnant contributions to break the degeneracy between spin-parity $1/2^-$ and $3/2^-$. That these effects are finally small can be seen in the breakup of the degeneracy of the $P_c(4440)$ and $P_c(4457)$ states recently observed in Ref. [2]. There are several works including pion exchange that break the degeneracy of the $1/2^-, 3/2^-$ states around this energy [83–86], but the small difference of mass between these states gives us an idea of the role played by π exchange in these cases. Uncertainties of this type in our predictions must certainly be admitted.

As to σ-exchange, it is empirically accounted for in some of the former works, but the strength is unknown. However, there is one way to make this exchange quantitative by going to the root of the σ meson as dynamically generated from the $\pi\pi$ interaction [87,88]. Indeed, in Ref. [89] the σ-exchange between nucleons was studied from the point of view of the exchange of two interacting mesons in s-wave. The same picture was used in the study of the meson-meson interaction describing the $Z_c(3980)$ [90] and $Z_c(4000)$ [91] and its effect was found minor. In particular, for meson–baryon interaction, the σ-exchange from this perspective was considered in Ref. [92] in the study of the $\bar{K}N$ interaction and it was found very much suppressed.

3 Results

3.1 Pseudoscalar-baryon ($1/2^+$) states, mixed symmetric sector

In Table 3, we consider the channels in this sector together with their threshold masses.[1]

In Table 4 we show the coefficients D_{ij} of Eq. (27). We find that there are some terms which go with λ. These terms involve the exchange of D^* and they are reduced.

[1] The masses of the states not reported in the PDG are taken from the quark model calculation of Ref. [51].

Table 3 Channels considered for sector $J^P = 1/2^-$ (MS)

Channel	$\Xi_{bc}\pi$	$\Xi_{bc}\eta$	$\Omega_{bc}K$	$\Sigma_b D$	$\Sigma_c \bar{B}$	$\Xi_b' D_s$	$\Xi_c' \bar{B}_s$
Threshold (MeV)	7057	7467	7482	7680	7733	7903	7945

Table 4 D_{ij} coefficients for sector $J^P = 1/2^-$ (MS)

$J^P = 1/2^-$	$\Xi_{bc}\pi$	$\Xi_{bc}\eta$	$\Omega_{bc}K$	$\Sigma_b D$	$\Sigma_c \bar{B}$	$\Xi_b' D_s$	$\Xi_c' \bar{B}_s$
$\Xi_{bc}\pi$	-2	0	$\sqrt{\frac{3}{2}}$	$\frac{1}{2}\lambda$	0	0	0
$\Xi_{bc}\eta$		0	$-\frac{2}{\sqrt{3}}$	$-\frac{1}{\sqrt{2}}\lambda$	0	$-\frac{1}{\sqrt{6}}\lambda$	0
$\Omega_{bc}K$			-1	0	0	$\frac{1}{\sqrt{2}}\lambda$	0
$\Sigma_b D$				-3	0	$\sqrt{3}$	0
$\Sigma_c \bar{B}$					-3	0	$\sqrt{3}$
$\Xi_b' D_s$						-1	~ 0
$\Xi_c' \bar{B}_s$							-1

Table 5 Poles for pesudoscalar-baryon (1/2) (MS) states (all units are in MeV)

$q_{\max}$	600	650	700	750	800
	7132.04+i104.00	7131.50+i95.13	7130.05+i86.36	7127.88+i77.57	7126.10+i68.25
	7434.02+i0.52	7372.22+i0.64	7305.50+i0.98	7235.38+i1.72	7162.72+i3.43
	7450.31	7372.55	7285.56	7190.26	7087.81

Table 6 The coupling constants to various channels and $g_i G_i^{II}$ in MeV with $q_{\max} = 650$ MeV

7131.50+i95.13	$\Xi_{bc}\pi$	$\Xi_{bc}\eta$	$\Omega_{bc}K$	$\Sigma_b D$
g_i	1.70+i1.23	$-0.03-$i0.10	$-0.85-$i0.74	$-0.67-$i0.40
$g_i G_i^{II}$	$-73.84-$i12.90	0.05+i0.64	4.46+i5.46	1.18+i0.96
	$\Sigma_c \bar{B}$	$\Xi_b' D_s$	$\Xi_c' \bar{B}_s$	
g_i	0	0.18+i0.19	0	
$g_i G_i^{II}$	0	$-0.22-$i0.29	0	

Table 7 The coupling constants to various channels and $g_i G_i^{II}$ in MeV with $q_{\max} = 650$ MeV

7372.22+i0.64	$\Xi_{bc}\pi$	$\Xi_{bc}\eta$	$\Omega_{bc}K$	$\Sigma_b D$
g_i	$-0.02+$i0.14	$0.27-$i0.03	$0.08-$i0.10	$9.40-$i0.02
$g_i G_i^{II}$	$-4.27-$i2.06	$-3.33+$i0.38	$-0.95+$i1.14	$-29.42+$i0.01
	$\Sigma_c \bar{B}$	$\Xi_b' D_s$	$\Xi_c' \bar{B}_s$	
g_i	0	$-5.19+$i0.01	0	
$g_i G_i^{II}$	0	$10.02-$i0.01	0	

The value of λ is the reduction factor versus the exchange of a light vector, which in Ref. [67] is found to be around $\lambda = 0.25$ as in Ref. [93]. Apart from that, when exchanging B_c meson we set the D_{ij} result as ~ 0, since it is highly suppressed.

In Table 5 the poles for three states that appear in this sector are shown for different values of the cutoff $q_{\max}$. As in former works we take $q_{\max} = 650$ MeV. In Tables 6 and 7 we take the first two states of Table 5 and show the couplings g_i, and the wave functions at the origin $g_i G_i$ (see Ref. [94]). We

Table 8 The coupling constants to various channels and $g_i G_i^{II}$ in MeV with $q_{\max} = 650$ MeV

7372.55	$\Xi_{bc}\pi$	$\Xi_{bc}\eta$	$\Omega_{bc}K$	$\Sigma_b D$
g_i	0	0	0	0
$g_i G_i^{II}$	0	0	0	0
	$\Sigma_c \bar{B}$	$\Xi_b' D_s$	$\Xi_c' \bar{B}_s$	
g_i	18.10	0	-10.17	
$g_i G_i^{II}$	-18.43	0	6.96	

Table 9 Channels considered for sector $J^P = 1/2^-$ (MA)

Channel	$\Xi_{bc}\pi$	$\Xi_{bc}\eta$	$\Omega_{bc}K$	$\Lambda_b D$	$\Lambda_c \bar{B}$	$\Xi_b D_s$	$\Xi_c \bar{B}_s$
Threshold (MeV)	7057	7467	7482	7487	7565	7761	7836

Table 10 D_{ij} coefficients for sector $J^P = 1/2^-$ (MA)

$J^P = 1/2^-$	$\Xi_{bc}\pi$	$\Xi_{bc}\eta$	$\Omega_{bc}K$	$\Lambda_b D$	$\Lambda_c \bar{B}$	$\Xi_b D_s$	$\Xi_c \bar{B}_s$
$\Xi_{bc}\pi$	-2	0	$\sqrt{\frac{3}{2}}$	$-\frac{\sqrt{3}}{2}\lambda$	0	0	0
$\Xi_{bc}\eta$		0	$-\frac{2}{\sqrt{3}}$	$-\frac{1}{\sqrt{6}}\lambda$	0	$\frac{1}{\sqrt{6}}\lambda$	0
$\Omega_{bc}K$			-1	0	0	$\frac{1}{\sqrt{2}}\lambda$	0
$\Lambda_b D$				-1	~ 0	-1	0
$\Lambda_c \bar{B}$					-1	0	-1
$\Xi_b D_s$						-1	~ 0
$\Xi_c \bar{B}_s$							-1

Table 11 Poles for pesudoscalar-baryon (1/2) (MA) states (all units are in MeV)

$q_{\max}$	600	650	700	750	800
	7131.20+i102.93	7130.33+i93.80	7128.44+i84.77	7125.60+i75.91	7121.84+i67.11
	7428.22+i0.52	7403.51+i0.93	7373.53+i1.52	7338.59+i2.35	7299.25+i3.59
	7492.72	7462.49	7425.33	7381.21	7330.34

Table 12 Coupling constants to various channels and $g_i G_i^{II}$ in MeV with $q_{\max} = 650$ MeV

7130.33+i93.80	$\Xi_{bc}\pi$	$\Xi_{bc}\eta$	$\Omega_{bc}K$	$\Lambda_b D$
g_i	1.70+i1.23	$-0.01-$i0.08	$-0.85-$i0.73	1.00+i0.42
$g_i G_i^{II}$	$-73.60-$i12.80	$-0.03+$i0.52	4.44+i5.35	$-2.45-$i1.67
	$\Lambda_c \bar{B}$	$\Xi_b D_s$	$\Xi_c \bar{B}_s$	
g_i	0	0.24+i0.23	0	
$g_i G_i^{II}$	0	$-0.35-$i0.43	0	

see that the first state at 7131 MeV has a large width of about 200 MeV and couples mostly to $\Xi_{bc}\pi$. However, the second state at 7372 MeV has a very narrow width and is basically a $\Sigma_b D$ bound state, although it also couples strongly to $\Xi'_b D_s$. The last state in Table 5 for $q_{\max} = 650$ MeV, appears at the same energy as the former one but the couplings are different as can be seen in Table 8.

As it can be seen in Table 5, the last two states in the row of $q_{\max} = 650$ MeV are less stable with the changes of $q_{\max}$ and, hence, more uncertain.

3.2 Pseudoscalar-baryon ($1/2^+$) states, mixed antisymmetric sector

We follow here the same pattern as in the former subsection with the mixed antisymmetric states. In Table 9 we show the channels and the threshold masses. In Table 10 we show the D_{ij} coefficients. In Table 11 we show the states (poles) found in this sector. We find three clear states, one with a large width of almost 200 MeV and two more states with very narrow widths. The first state is actually the same one that we found before, because it couples mostly to $\Xi_{bc}\pi$ as shown in Table 12, and this state appears with MS and MA spins. However, the second state couples mostly to $\Lambda_b D$ and $\Xi_b D_s$ as shown in Table 13, and is then a different state. The state at 7462 MeV couples mostly to $\Lambda_c \bar{B}$ and $\Xi_c \bar{B}_s$, as shown in Table 14.

3.3 Vector–baryon ($1/2^+$) states, mixed symmetric sector

We show in Table 15 the channels and the thresholds that in this case give rise to degenerate states in sector $J^P = 1/2^-, 3/2^-$. The D_{ij} coefficients are shown in Table 16 and in Table 17 we find four states, three of them with zero width and the last one with a large width. In Tables 18, 19 20 and 21 we show the couplings and wave functions of these states. The state at 7418 MeV could be regarded as a $\Sigma_c \bar{B}^*$ bound state, but it also couples strongly to $\Xi'_c \bar{B}^*_s$. The state at 7501 MeV could be identified with a $\Sigma_b D^*$ state, the one at 7595 MeV as a $\Xi_{bc}\rho$ bound state, and the state at 7837 MeV and $\Gamma \simeq 180$ MeV corresponds to a $\Omega_{bc}K^*$ bound state which decays strongly in $\Xi_{bc}\omega$.

Table 13 Coupling constants to various channels and $g_i G_i^{II}$ in MeV with $q_{\max} = 650$ MeV

7403.51+i0.93	$\Xi_{bc}\pi$	$\Xi_{bc}\eta$	$\Omega_{bc}K$	$\Lambda_b D$
g_i	0.02−i0.17	0.24+i0.05	0.25+i0.13	4.06−i0.05
$g_i G_i^{II}$	5.42+i1.92	−3.40−i0.75	−3.35−i1.72	−30.28+i0.20
	$\Lambda_c \bar{B}$	$\Xi_b D_s$	$\Xi_c \bar{B}_s$	
g_i	0	3.85−i0.05	0	
$g_i G_i^{II}$	0	−10.26+i0.11	0	

Table 14 Coupling constants to various channels and $g_i G_i^{II}$ in MeV with $q_{\max} = 650$ MeV

7462.49	$\Xi_{bc}\pi$	$\Xi_{bc}\eta$	$\Omega_{bc}K$	$\Lambda_b D$
g_i	0	0	0	0
$g_i G_i^{II}$	0	0	0	0
	$\Lambda_c \bar{B}$	$\Xi_b D_s$	$\Xi_c \bar{B}_s$	
g_i	7.46	0	7.19	
$g_i G_i^{II}$	−18.58	0	−7.01	

3.4 Vector–baryon $(1/2^+)$, mixed antisymmetric sector

In Table 22 we show the coupled channels and the thresholds and in Table 23 we show the D_{ij} coefficients. The states are shown in Table 24. The couplings of the states to the different channels are shown in Tables 25, 26, 27 and 28. The 7599 MeV and 7826 MeV states are basically the same states as before because the dominant channel and decay channel appear in both the MS and MA representations.

3.5 Pseudoscalar-baryon $(3/2)^+$ states

In this case the spin wave function, χ_S, is full symmetric and the states generated are in the sector $J^P = 3/2^-$. In Table 29 we show the channels and the thresholds and in Table 30 the D_{ij} coefficients. In Table 31 we show the states obtained for different values of the cut off. We observe three states, one with a width of about 190 MeV and the other two narrow. Inspecting Tables 32, 33, 34 we can see that the first state couples strongly to $\Xi_{bc}^*\pi$, which is open, and this is the reason for the large width. The second state couples mostly to $\Sigma_b^* D$ and the third one to $\Sigma_c^* \bar{B}$.

Table 15 Channels considered for sector $J^P = 1/2^-, 3/2^-$ (MS)

Channel	$\Xi_{bc}\rho$	$\Xi_{bc}\omega$	$\Sigma_c \bar{B}^*$	$\Sigma_b D^*$	$\Omega_{bc}K^*$	$\Xi_{bc}\phi$	$\Xi_c' \bar{B}_s^*$	$\Xi_b' D_s^*$
Threshold (MeV)	7694	7702	7779	7822	7882	7938	7993	8047

Table 16 D_{ij} coefficients for sector $J^P = 1/2^-, 3/2^-$ (MS)

$J^P = 1/2^-, 3/2^-$	$\Xi_{bc}\rho$	$\Xi_{bc}\omega$	$\Sigma_c \bar{B}^*$	$\Sigma_b D^*$	$\Omega_{bc}K^*$	$\Xi_{bc}\phi$	$\Xi_c' \bar{B}_s^*$	$\Xi_b' D_s^*$
$\Xi_{bc}\rho$	−2	0	0	$\frac{1}{2}\lambda$	$\sqrt{\frac{3}{2}}$	0	0	0
$\Xi_{bc}\omega$		0	0	$-\frac{\sqrt{3}}{2}\lambda$	$-\frac{1}{\sqrt{2}}$	0	0	0
$\Sigma_c \bar{B}^*$			−3	0	0	0	$\sqrt{3}$	0
$\Sigma_b D^*$				−3	0	0	0	$\sqrt{3}$
$\Omega_{bc}K^*$					−1	1	0	$\frac{1}{\sqrt{2}}\lambda$
$\Xi_{bc}\phi$						0	0	$\frac{1}{\sqrt{2}}\lambda$
$\Xi_c' \bar{B}_s^*$							−1	0
$\Xi_b' D_s^*$								−1

Table 17 Poles for vector–baryon (1/2) (MS) states (all units are in MeV)

$q_{\max}$	600	650	700	750	800
	7496.28	7418.47	7331.40	7236.01	7133.42
	7565.71	7501.56	7431.85	7358.22	7282.17
	7619.74	7595.24	7569.14	7541.98	7514.40
	7861.84+i93.45	7837.81+i91.45	7810.81+86.76	7784.37+i79.86	7758.25+i70.40

Table 18 Coupling constants to various channels and $g_i G_i^{II}$ in MeV with $q_{\max} = 650$ MeV

7418.47	$\Xi_{bc}\rho$	$\Xi_{bc}\omega$	$\Sigma_c \bar{B}^*$	$\Sigma_b D^*$
g_i	0	0	18.18	0
$g_i G_i^{II}$	0	0	−18.36	0
	$\Omega_{bc} K^*$	$\Xi_{bc}\phi$	$\Xi_c' \bar{B}_s^*$	$\Xi_b' D_s^*$
g_i	0	0	−10.22	0
$g_i G_i^{II}$	0	0	6.91	0

Table 19 Coupling constants to various channels and $g_i G_i^{II}$ in MeV with $q_{\max} = 650$ MeV

7501.56	$\Xi_{bc}\rho$	$\Xi_{bc}\omega$	$\Sigma_c \bar{B}^*$	$\Sigma_b D^*$
g_i	−0.62	0.44	0	9.91
$g_i G_i^{II}$	4.76	−3.28	0	−28.37
	$\Omega_{bc} K^*$	$\Xi_{bc}\phi$	$\Xi_c' \bar{B}_s^*$	$\Xi_b' D_s^*$
g_i	0.41	0.05	0	−5.47
$g_i G_i^{II}$	−1.85	−0.18	0	9.72

Table 20 Coupling constants to various channels and $g_i G_i^{II}$ in MeV with $q_{\max} = 650$ MeV

7595.24	$\Xi_{bc}\rho$	$\Xi_{bc}\omega$	$\Sigma_c \bar{B}^*$	$\Sigma_b D^*$
g_i	3.58	−0.28	0	1.03
$g_i G_i^{II}$	−38.74	2.93	0	−3.84
	$\Omega_{bc} K^*$	$\Xi_{bc}\phi$	$\Xi_c' \bar{B}_s^*$	$\Xi_b' D_s^*$
g_i	−2.36	0.50	0	−0.66
$g_i G_i^{II}$	13.01	−2.24	0	1.38

4 Wave functions

It is interesting to see how are the wave functions that we have generated. They are a bit different than ordinary wave functions with local potentials decreasing very rapidly as $r \to \infty$. In order to see that, we have to go back to the work of Ref. [94], where we find that the use of Eq. (28) with a G function regularized with a cut off $q_{\max}$ is equivalent to solving the Lippmann–Schwinger equation with a potential

$$V(\vec{q}, \vec{q}^{\,'}) = V\,\theta(q_{\max} - |\vec{q}\,|)\,\theta(q_{\max} - |\vec{q}^{\,'}|), \tag{33}$$

which is a non-local potential. The wave function in momentum space is particularly easy (see Eqs. (34), (47) of Ref. [94] and Eq. (105) of Ref. [95] generalizing to relativistic energies)

$$\langle \vec{q}\,|\psi\rangle = g\,\frac{\theta(q_{\max} - |\vec{q}\,|)}{E - w_1(\vec{q}\,) - w_2(\vec{q}\,)}, \tag{34}$$

where $w_i(\vec{q}\,) = \sqrt{m_i^2 + \vec{q}^{\,2}}$ and g is the coupling of the wave function to the channel with particles 1 and 2.

The wave function in coordinate space is given by

$$\begin{aligned}\langle \vec{x}\,|\psi\rangle &= \int \frac{d^3q}{(2\pi)^{3/2}}\, e^{i\vec{q}\cdot\vec{x}}\,\langle \vec{q}\,|\psi\rangle \\ &= \frac{2\pi}{(2\pi)^{3/2}}\, g\,\frac{2}{r}\int_0^{q_{\max}} q\,dq\,\frac{1}{E - w_1(\vec{q}\,) - w_2(\vec{q}\,)}\,\sin(qr).\end{aligned} \tag{35}$$

It is interesting to note that unlike in ordinary potentials, which could be simulated with $q_{\max} \to \infty$ and $w_1(\vec{q}\,) + w_2(\vec{q}\,)$ and $\sin(qr)$ providing convergence in the q integration, in our case $q_{\max} = 650$ MeV corresponds to a value where $\vec{q}^{\,2}/m_i^2$ is very small and the $w_1(\vec{q}\,) + w_2(\vec{q}\,)$ term does not help in the convergence of the integral, which is determined by $q_{\max}$. One can then see that the shape of the wave function does not depend much on E, which diverts from ordinary wave functions with a rapidly decreasing local potential where the size is roughly given by $r = 1/\sqrt{2\mu B}$, with μ the reduced mass and B the binding. We show this in an example of a very bound component, the 7372 MeV state of Table 7, which couples mostly to $\Sigma_b D$.

In Fig. 2 we show the wave function corresponding to this channel. While naively we would expect a size of around 0.2 fm according to the intuitive formula, we find that the wave function extends much further and even at $r \simeq 1$ fm is not

Table 21 Coupling constants to various channels and $g_i G_i^{II}$ in MeV with $q_{\max} = 650$ MeV

7837.81+i91.45	$\Xi_{bc}\rho$	$\Xi_{bc}\omega$	$\Sigma_c \bar{B}^*$	$\Sigma_b D^*$
g_i	0.04+i0.49	1.42+i0.49	0	−0.05+i0.01
$g_i G_i^{II}$	−24.78−i9.65	−58.19+i55.70	0	1.86−i2.19
	$\Omega_{bc} K^*$	$\Xi_{bc}\phi$	$\Xi_c' \bar{B}_s^*$	$\Xi_b' D_s^*$
g_i	3.45−i1.23	−2.07−i0.61	0	0.14−i0.57
$g_i G_i^{II}$	−40.99−i8.16	14.22+i12.01	0	−1.13+i1.81

Table 22 Channels considered for sector $J^P = 1/2^-, 3/2^-$ (MA)

Channel	$\Lambda_c \bar{B}^*$	$\Lambda_b D^*$	$\Xi_{bc}\rho$	$\Xi_{bc}\omega$	$\Omega_{bc} K^*$	$\Xi_c \bar{B}_s^*$	$\Xi_b D_s^*$	$\Xi_{bc}\phi$
Threshold (MeV)	7611	7629	7694	7702	7882	7884	7905	7938

Table 23 D_{ij} coefficients for sector $J^P = 1/2^-, 3/2^-$ (MA)

$J^P = 1/2^-, 3/2^-$	$\Lambda_c\bar{B}^*$	$\Lambda_b D^*$	$\Xi_{bc}\rho$	$\Xi_{bc}\omega$	$\Omega_{bc}K^*$	$\Xi_c\bar{B}_s^*$	$\Xi_b D_s^*$	$\Xi_{bc}\phi$
$\Lambda_c\bar{B}^*$	-1	~ 0	0	0	0	-1	0	0
$\Lambda_b D^*$		-1	$-\frac{\sqrt{3}}{2}\lambda$	$-\frac{1}{2}\lambda$	0	0	-1	0
$\Xi_{bc}\rho$			-2	0	$\sqrt{\frac{3}{2}}$	0	0	0
$\Xi_{bc}\omega$				0	$-\frac{1}{\sqrt{2}}$	0	0	0
$\Omega_{bc}K^*$					-1	0	$\frac{1}{\sqrt{2}}\lambda$	1
$\Xi_c\bar{B}_s^*$						-1	~ 0	0
$\Xi_b D_s^*$							-1	$-\frac{1}{\sqrt{2}}\lambda$
$\Xi_{bc}\phi$								0

Table 24 Poles for vector–baryon (1/2) (MA) states (all units are in MeV)

$q_{\max}$	600	650	700	750	800
	7538.75	7508.55	7471.42	7427.31	7376.44
	7559.38	7531.22	7497.76	7459.40	7416.60
	7621.95	7599.65	7575.06	7548.85	7521.72
	7853.18+i80.53	7826.83+i77.82	7798.50+i72.97	7769.94+i65.32	7740.93+i54.42

Table 25 Coupling constants to various channels and $g_i G_i^{II}$ in MeV with $q_{\max} = 650$ MeV

7508.55	$\Lambda_c\bar{B}^*$	$\Lambda_b D^*$	$\Xi_{bc}\rho$	$\Xi_{bc}\omega$
g_i	7.49	0	0	0
$g_i G_i^{II}$	-18.51	0	0	0
	$\Omega_{bc}K^*$	$\Xi_c\bar{B}_s^*$	$\Xi_b D_s^*$	$\Xi_{bc}\phi$
g_i	0	7.22	0	0
$g_i G_i^{II}$	0	-6.94	0	0

Table 26 Coupling constants to various channels and $g_i G_i^{II}$ in MeV with $q_{\max} = 650$ MeV

7531.22	$\Lambda_c\bar{B}^*$	$\Lambda_b D^*$	$\Xi_{bc}\rho$	$\Xi_{bc}\omega$
g_i	0	4.32	1.43	0.18
$g_i G_i^{II}$	0	-28.22	-12.03	-1.44
	$\Omega_{bc}K^*$	$\Xi_c\bar{B}_s^*$	$\Xi_b D_s^*$	$\Xi_{bc}\phi$
g_i	-0.71	0	3.97	0.23
$g_i G_i^{II}$	3.38	0	-9.64	-0.90

Table 27 Coupling constants to various channels and $g_i G_i^{II}$ in MeV with $q_{\max} = 650$ MeV

7599.65	$\Lambda_c\bar{B}^*$	$\Lambda_b D^*$	$\Xi_{bc}\rho$	$\Xi_{bc}\omega$
g_i	0	-0.74	3.35	-0.42
$g_i G_i^{II}$	0	8.59	-36.94	4.55
	$\Omega_{bc}K^*$	$\Xi_c\bar{B}_s^*$	$\Xi_b D_s^*$	$\Xi_{bc}\phi$
g_i	-2.30	0	-1.07	0.44
$g_i G_i^{II}$	12.79	0	3.05	-1.99

negligible. This can be better appreciated in Fig. 3 where we plot the wave function squared times r^2. We see that it peaks around 0.7 fm and still has a sizable strength around 1 fm and beyond.

5 Conclusions

We have studied the meson–baryon interaction in the sector corresponding to Ξ_{bc} quantum numbers. We take the cou-

Table 28 Coupling constants to various channels and $g_i G_i^{II}$ in MeV with $q_{\max} = 650$ MeV

7826.83+i77.82	$\Lambda_c\bar{B}^*$	$\Lambda_b D^*$	$\Xi_{bc}\rho$	$\Xi_{bc}\omega$
g_i	0	-0.09+i0.03	0.11+i0.47	1.36+i0.40
$g_i G_i^{II}$	0	$-1.43-$i8.14	$-23.63-$i5.98	-50.30+i49.92
	$\Omega_{bc}K^*$	$\Xi_c\bar{B}_s^*$	$\Xi_b D_s^*$	$\Xi_{bc}\phi$
g_i	3.23$-$i1.05	0	-1.87+i0.13	$-2.07-$i0.51
$g_i G_i^{II}$	$-38.27-$i5.14	0	10.68+i4.71	15.03+i9.96

Table 29 Channels considered for sector $J^P = 3/2^-$ (S)

Channel	$\Xi_{bc}^*\pi$	$\Xi_{bc}^*\eta$	Ω_{bc}^*K	Σ_b^*D	$\Sigma_c^*\bar{B}$	$\Xi_b^*D_s$	$\Xi_c^*\bar{B}_s$
Threshold (MeV)	7124	7534	7542	7701	7797	7921	8013

Table 30 D_{ij} coefficients for sector $J^P = 3/2^-$ (S)

$J^P = 3/2^-$	$\Xi_{bc}^*\pi$	$\Xi_{bc}^*\eta$	Ω_{bc}^*K	Σ_b^*D	$\Sigma_c^*\bar{B}$	$\Xi_b^*D_s$	$\Xi_c^*\bar{B}_s$
$\Xi_{bc}^*\pi$	-2	0	$\sqrt{\frac{3}{2}}$	$\frac{1}{2}\lambda$	0	0	0
$\Xi_{bc}^*\eta$		0	$-\frac{2}{\sqrt{3}}$	$-\frac{1}{\sqrt{2}}\lambda$	0	$-\frac{1}{\sqrt{6}}\lambda$	0
Ω_{bc}^*K			-1	0	0	$\frac{1}{\sqrt{2}}\lambda$	0
Σ_b^*D				-3	0	$\sqrt{3}$	0
$\Sigma_c^*\bar{B}$					-3	0	$\sqrt{3}$
$\Xi_b^*D_s$						-1	0
$\Xi_c^*\bar{B}_s$							-1

Table 31 Poles for pesudoscalar-baryon (3/2) (S) states (all units are in MeV)

$q_{\max}$	600	650	700	750	800
	7198.92+i103.55	7198.33+i94.56	7196.86+i85.55	7195.05+i76.23	7195.23+i68.21
	7455.11+i0.49	7393.03+i0.76	7326.17+i1.31	7531.93+i7.50	7180.43+i2.88
	7513.15	7434.97	7347.43	7251.46	7148.17

Table 32 Coupling constants to various channels and $g_i G_i^{II}$ in MeV with $q_{\max} = 650$ MeV

7198.33+i94.56	$\Xi_{bc}^*\pi$	$\Xi_{bc}^*\eta$	Ω_{bc}^*K	Σ_b^*D
g_i	1.70+i1.23	$-0.03-$i0.11	$-0.87-$i0.74	$-0.74-$i0.50
$g_i G_i^{II}$	$-73.77-$i12.77	0.06+i0.68	4.63+i5.57	1.36+i1.27
	$\Sigma_c^*\bar{B}$	$\Xi_b^*D_s$	$\Xi_c^*\bar{B}_s$	
g_i	0	0.21+i0.25	0	
$g_i G_i^{II}$	0	$-0.26-$i0.40	0	

Table 33 Coupling constants to various channels and $g_i G_i^{II}$ in MeV with $q_{\max} = 650$ MeV

7393.03+i0.76	$\Xi_{bc}^*\pi$	$\Xi_{bc}^*\eta$	Ω_{bc}^*K	Σ_b^*D
g_i	$-0.02+$i0.16	$0.25-$i0.03	$0.05-$i0.10	$9.41-$i0.03
$g_i G_i^{II}$	$-4.32-$i2.86	$-2.60+$i0.27	$-0.54+$i1.07	$-29.44+$i0.04
	$\Sigma_c^*\bar{B}$	$\Xi_b^*D_s$	$\Xi_c^*\bar{B}_s$	
g_i	0	$-5.21+$i0.01	0	
$g_i G_i^{II}$	0	$10.10-$i0.01	0	

Table 34 Coupling constants to various channels and $g_i G_i^{II}$ in MeV with $q_{\max} = 650$ MeV

7434.97	$\Xi_{bc}^*\pi$	$\Xi_{bc}^*\eta$	Ω_{bc}^*K	Σ_b^*D
g_i	0	0	0	0
$g_i G_i^{II}$	0	0	0	0
	$\Sigma_c^*\bar{B}$	$\Xi_b^*D_s$	$\Xi_c^*\bar{B}_s$	
g_i	18.14	0	-10.20	
$g_i G_i^{II}$	-18.47	0	6.94	

pled channels that can lead to these quantum numbers and study their interaction in s-wave. The model used for the interaction is based on an extrapolation of the local hidden gauge approach, which uses vector exchange as the source of interaction. The dominant terms come from the exchange of light vector mesons which render the heavy quarks as spectators and the approach automatically satisfies the heavy quark symmetry rules. The interaction is properly unitarized in coupled channels and by looking at poles in the second Riemann sheet we look for the states of the

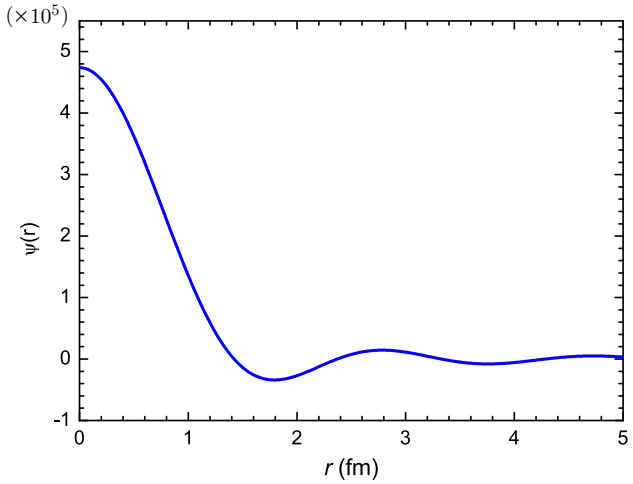

Fig. 2 Wave function $\Psi(r)$ corresponding to channel $\Sigma_b D$

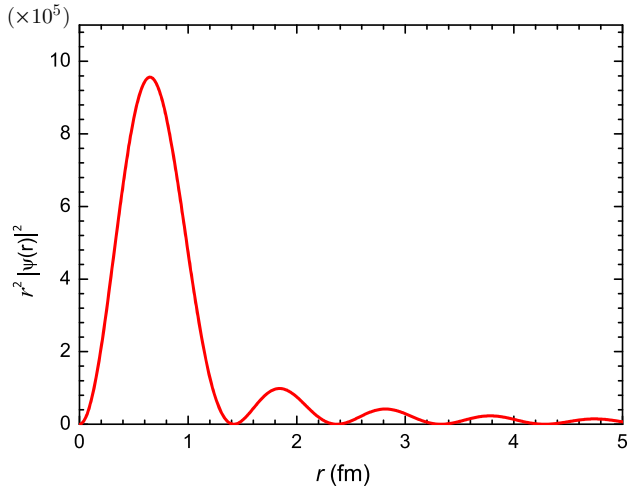

Fig. 3 The function $r^2\,|\Psi(r)|^2$ corresponding to channel $\Sigma_b D$

system. We consider the interaction of pseudoscalars with baryons of $J^P = 1/2^+, 3/2^+$ and of vectors with baryons of $J^P = 1/2^+$ and distinguish spin mixed symmetric and mixed antisymmetric states in analogy to the Ξ and Ξ' states. We find several states which correspond to bound meson–baryon states with zero or small widths and a few that have a large width, Since the input used to generate these states is the same one used to study Ω_c and states of hidden charm, which produced results in excellent agreement with experiment, we have confidence that the predictions made are realistic and encourage the experimental search of such states. In some cases the main decay channels have been identified and this can be useful in the planning of experimental proposals.

Acknowledgements We thank the hospitality of Guangxi Normal University where the main part of this work is done. Qi-Xin Yu acknowledges the support from the National Natural Science Foundation of China (Grant nos. 11775024, 11575023 and 11805153) and China Scholarship Council. This work is partly supported by the National Natural Science Foundation of China under Grants nos. 11975083, 11847317 and 11565007. This work is partly supported by the Spanish Ministerio de Economia y Competitividad and European FEDER funds under Contracts No. FIS2017-84038-C2-1-P B and No. FIS2017-84038-C2-2-P B, and the Generalitat Valenciana in the program Prometeo II-2014/068, and the project Severo Ochoa of IFIC, SEV-2014-0398.

Data Availability Statement This manuscript has no associated data or the data will not be deposited. [Authors' comment: All data generated during this study are contained in this published article.]

Funded by SCOAP[3].

References

1. R. Aaij et al. [LHCb Collaboration], Phys. Rev. Lett. **115**, 072001 (2015)
2. R. Aaij et al. [LHCb Collaboration], Phys. Rev. Lett. **122**(22), 222001 (2019)
3. R. Aaij et al. [LHCb Collaboration], Phys. Rev. Lett. **118**(18), 182001 (2017)
4. R. Aaij et al. [LHCb Collaboration], Phys. Rev. Lett. **119**(11), 112001 (2017)
5. A. De Rujula, H. Georgi, S.L. Glashow, Phys. Rev. D **12**, 147 (1975)
6. D. Ebert, R.N. Faustov, V.O. Galkin, A.P. Martynenko, Phys. Rev. D **66**, 014008 (2002)
7. J.G. Körner, M. Kramer, D. Pirjol, Prog. Part. Nucl. Phys. **33**, 787 (1994)
8. H.X. Chen, W. Chen, X. Liu, Y.R. Liu, S.L. Zhu, Rep. Prog. Phys. **80**(7), 076201 (2017)
9. F.S. Yu, H.Y. Jiang, R.H. Li, C.D. Lü, W. Wang, Z.X. Zhao, Chin. Phys. C **42**(5), 051001 (2018)
10. W. Wang, F.S. Yu, Z.X. Zhao, Eur. Phys. J. C **77**(11), 781 (2017)
11. W. Wang, Z.P. Xing, J. Xu, Eur. Phys. J. C **77**(11), 800 (2017)
12. T. Gutsche, M.A. Ivanov, J.G. Körner, V.E. Lyubovitskij, Phys. Rev. D **96**(5), 054013 (2017)
13. N. Sharma, R. Dhir, Phys. Rev. D **96**(11), 113006 (2017)
14. X.H. Hu, Y.L. Shen, W. Wang, Z.X. Zhao, Chin. Phys. C **42**(12), 123102 (2018)
15. Y.J. Shi, W. Wang, Y. Xing, J. Xu, Eur. Phys. J. C **78**(1), 56 (2018)
16. M. Karliner, J.L. Rosner, Phys. Rev. D **97**(9), 094006 (2018)
17. Z.X. Zhao, Eur. Phys. J. C **78**(9), 756 (2018)
18. Z.P. Xing, Z.X. Zhao, Phys. Rev. D **98**(5), 056002 (2018)
19. Z.G. Wang, Eur. Phys. J. C **78**(10), 826 (2018)
20. H.Y. Cheng, Y.L. Shi, Phys. Rev. D **98**(11), 113005 (2018)
21. L.J. Jiang, B. He, R.H. Li, Eur. Phys. J. C **78**(11), 961 (2018)
22. Q.A. Zhang, Eur. Phys. J. C **78**(12), 1024 (2018)
23. T. Gutsche, M.A. Ivanov, J.G. Körner, V.E. Lyubovitskij, Z. Tyulemissov, Phys. Rev. D **99**(5), 056013 (2019)
24. A.K. Ridgway, M.B. Wise, Phys. Lett. B **793**, 181 (2019)

25. H.Y. Cheng, F. Xu, Phys. Rev. D **99**(7), 073006 (2019)
26. A.S. Gerasimov, A.V. Luchinsky, arXiv:1905.11740 [hep-ph]
27. H.S. Li, L. Meng, Z.W. Liu, S.L. Zhu, Phys. Lett. B **777**, 169 (2018)
28. L.Y. Xiao, K.L. Wang, Q. Lu, X.H. Zhong, S.L. Zhu, Phys. Rev. D **96**(9), 094005 (2017)
29. T. Mehen, Phys. Rev. D **96**(9), 094028 (2017)
30. E.L. Cui, H.X. Chen, W. Chen, X. Liu, S.L. Zhu, Phys. Rev. D **97**(3), 034018 (2018)
31. L.Y. Xiao, Q.F. Lü, S.L. Zhu, Phys. Rev. D **97**(7), 074005 (2018)
32. H. Bahtiyar, K.U. Can, G. Erkol, M. Oka, T.T. Takahashi, Phys. Rev. D **98**(11), 114505 (2018)
33. H.S. Li, L. Meng, Z.W. Liu, S.L. Zhu, Phys. Rev. D **96**(7), 076011 (2017)
34. L. Meng, H.S. Li, Z.W. Liu, S.L. Zhu, Eur. Phys. J. C **77**(12), 869 (2017)
35. U. Özdem, J. Phys. G **46**(3), 035003 (2019)
36. U. Özdem, arXiv:1906.08353 [hep-ph]
37. C.Y. Wang, C. Meng, Y.Q. Ma, K.T. Chao, Phys. Rev. D **99**(1), 014018 (2019)
38. Z.G. Wang, Eur. Phys. J. C **78**(4), 300 (2018)
39. K. Azizi, Y. Sarac, H. Sundu, Phys. Rev. D **98**(5), 054002 (2018)
40. T.M. Aliev, S. Bilmis, Nucl. Phys. A **984**, 99 (2019)
41. Y.J. Shi, W. Wang, Z.X. Zhao, arXiv:1902.01092 [hep-ph]
42. Y.J. Shi, Y. Xing, Z.X. Zhao, Eur. Phys. J. C **79**(6), 501 (2019)
43. N. Mathur, M. Padmanath, Phys. Rev. D **99**(3), 031501 (2019)
44. V.V. Kiselev, A.V. Berezhnoy, A.K. Likhoded, Phys. Atom. Nucl. **81**(3), 369 (2018) [Yad. Fiz. **81**(3), 356 (2018)]
45. Q.F. Lü, K.L. Wang, L.Y. Xiao, X.H. Zhong, Phys. Rev. D **96**(11), 114006 (2017)
46. Z. Shah, A.K. Rai, Eur. Phys. J. A **53**(10), 195 (2017)
47. Q.S. Zhou, K. Chen, X. Liu, Y.R. Liu, S.L. Zhu, Phys. Rev. C **98**(4), 045204 (2018)
48. X.Z. Weng, X.L. Chen, W.Z. Deng, Phys. Rev. D **97**(5), 054008 (2018)
49. J.M. Richard, A. Valcarce, J. Vijande, Phys. Rev. C **97**(3), 035211 (2018)
50. Q. Li, C.H. Chang, S.X. Qin, G.L. Wang, arXiv:1903.02282 [hep-ph]
51. C. Albertus, E. Hernandez, J. Nieves, J.M. Verde-Velasco, Eur. Phys. J. A **32**, 183 (2007) [Erratum: Eur. Phys. J. A **36**, 119 (2008)]
52. Z. Shah, A.K. Rai, Eur. Phys. J. C **77**(2), 129 (2017)
53. Y.L. Ma, M. Harada, J. Phys. G **45**(7), 075006 (2018)
54. M.Z. Liu, T.W. Wu, J.J. Xie, M. Pavon Valderrama, L.S. Geng, Phys. Rev. D **98**(1), 014014 (2018)
55. T.C. Mehen, A. Mohapatra, Phys. Rev. D **100**(7), 076014 (2019)
56. Z.H. Guo, Phys. Rev. D **96**(7), 074004 (2017)
57. M.J. Yan, X.H. Liu, S. González-Solís, F.K. Guo, C. Hanhart, U.G. Meißner, B.S. Zou, Phys. Rev. D **98**(9), 091502 (2018)
58. L. Meng, S.L. Zhu, Phys. Rev. D **100**(1), 014006 (2019)
59. R. Chen, A. Hosaka, X. Liu, Phys. Rev. D **96**(11), 114030 (2017)
60. D.L. Yao, Phys. Rev. D **97**(3), 034012 (2018)
61. A.N. Hiller Blin, Z.F. Sun, M.J. Vicente Vacas, Phys. Rev. D **98**(5), 054025 (2018)
62. Q.X. Yu, X.H. Guo, Nucl. Phys. B **947**, 114727 (2019)
63. S.L. Olsen, T. Skwarnicki, D. Zieminska, Rev. Mod. Phys. **90**(1), 015003 (2018)
64. M. Karliner, J.L. Rosner, T. Skwarnicki, Annu. Rev. Nucl. Part. Sci. **68**, 17 (2018)
65. Y.R. Liu, H.X. Chen, W. Chen, X. Liu, S.L. Zhu, Prog. Part. Nucl. Phys. **107**, 237 (2019)
66. J.M. Dias, V.R. Debastiani, J.-J. Xie, E. Oset, Phys. Rev. D **98**(9), 094017 (2018)
67. V.R. Debastiani, J.M. Dias, W.H. Liang, E. Oset, Phys. Rev. D **97**(9), 094035 (2018)
68. S. Sakai, L. Roca, E. Oset, Phys. Rev. D **96**(5), 054023 (2017)
69. M. Bando, T. Kugo, S. Uehara, K. Yamawaki, T. Yanagida, Phys. Rev. Lett. **54**, 1215 (1985)
70. M. Bando, T. Kugo, K. Yamawaki, Phys. Rep. **164**, 217 (1988)
71. U.G. Meißner, Phys. Rep. **161**, 213 (1988)
72. H. Nagahiro, L. Roca, A. Hosaka, E. Oset, Phys. Rev. D **79**, 014015 (2009)
73. G. Ecker, J. Gasser, H. Leutwyler, A. Pich, E. de Rafael, Phys. Lett. B **223**, 425 (1989)
74. G. Montaña, A. Feijoo, À. Ramos, Eur. Phys. J. A **54**(4), 64 (2018)
75. C.W. Xiao, J. Nieves, E. Oset, Phys. Rev. D **100**(1), 014021 (2019)
76. M.Z. Liu, Y.W. Pan, F.Z. Peng, M. Sánchez Sánchez, L.S. Geng, A. Hosaka, M. Pavon Valderrama, Phys. Rev. Lett. **122**(24), 242001 (2019)
77. Q.X. Yu, R. Pavao, V.R. Debastiani, E. Oset, Eur. Phys. J. C **79**(2), 167 (2019)
78. W.H. Liang, J.M. Dias, V.R. Debastiani, E. Oset, Nucl. Phys. B **930**, 524 (2018)
79. F.E. Close, *An introduction to quarks and partons* (Academic Press, Cambrige, 1979)
80. Z.F. Sun, J. He, X. Liu, Z.G. Luo, S.L. Zhu, Phys. Rev. D **84**, 054002 (2011)
81. W.H. Liang, T. Uchino, C.W. Xiao, E. Oset, Eur. Phys. J. A **51**(2), 16 (2015)
82. T. Uchino, W.H. Liang, E. Oset, Eur. Phys. J. A **52**(3), 43 (2016)
83. J. He, Eur. Phys. J. C **79**(5), 393 (2019)
84. R. Chen, Z.F. Sun, X. Liu, S.L. Zhu, Phys. Rev. D **100**(1), 011502 (2019)
85. M. Pavon Valderrama, Phys. Rev. D **100**(9), 094028 (2019)
86. M.Z. Liu, T.W. Wu, M. Sánchez Sánchez, M.P. Valderrama, L.S. Geng, J.J. Xie, arXiv:1907.06093 [hep-ph]
87. J.A. Oller, E. Oset, Nucl. Phys. A **620**, 438 (1997) [Erratum: Nucl. Phys. A **652**, 407 (1999)]
88. J.R. Pelaez, Phys. Rep. **658**, 1 (2016)
89. E. Oset, H. Toki, M. Mizobe, T.T. Takahashi, Prog. Theor. Phys. **103**, 351 (2000)
90. F. Aceti, M. Bayar, E. Oset, A. Martinez Torres, K.P. Khemchandani, J.M. Dias, F.S. Navarra, M. Nielsen, Phys. Rev. D **90**(1), 016003 (2014)
91. F. Aceti, M. Bayar, J.M. Dias, E. Oset, Eur. Phys. J. A **50**, 103 (2014)
92. A. Martinez Torres, K.P. Khemchandani, E. Oset, Eur. Phys. J. A **36**, 211 (2008)
93. T. Mizutani, A. Ramos, Phys. Rev. C **74**, 065201 (2006)
94. D. Gamermann, J. Nieves, E. Oset, E. Ruiz Arriola, Phys. Rev. D **81**, 014029 (2010)
95. J. Yamagata-Sekihara, J. Nieves, E. Oset, Phys. Rev. D **83**, 014003 (2011)